

A High Power Buckypaper Biofuel Cell: Exploiting 1,10-Phenanthroline-5,6-dione with FAD-Dependent Dehydrogenase for Catalytically-Powerful Glucose Oxidation

Andrew J. Gross, Xiaohong Chen, Fabien Giroud, Caroline Abreu, Alan Le Goff, Michael Holzinger, Serge Cosnier

▶ **To cite this version:**

Andrew J. Gross, Xiaohong Chen, Fabien Giroud, Caroline Abreu, Alan Le Goff, et al.. A High Power Buckypaper Biofuel Cell: Exploiting 1,10-Phenanthroline-5,6-dione with FAD-Dependent Dehydrogenase for Catalytically-Powerful Glucose Oxidation. ACS Catalysis, 2017, 7 (7), pp.4408 - 4416. 10.1021/acscatal.7b00738 . hal-01616374

HAL Id: hal-01616374

https://hal.univ-grenoble-alpes.fr/hal-01616374

Submitted on 19 Nov 2020

HAL is a multi-disciplinary open access archive for the deposit and dissemination of scientific research documents, whether they are published or not. The documents may come from teaching and research institutions in France or abroad, or from public or private research centers.

L'archive ouverte pluridisciplinaire **HAL**, est destinée au dépôt et à la diffusion de documents scientifiques de niveau recherche, publiés ou non, émanant des établissements d'enseignement et de recherche français ou étrangers, des laboratoires publics ou privés.

ACS Catalysis

Research Article

pubs.acs.org/acscatalysis

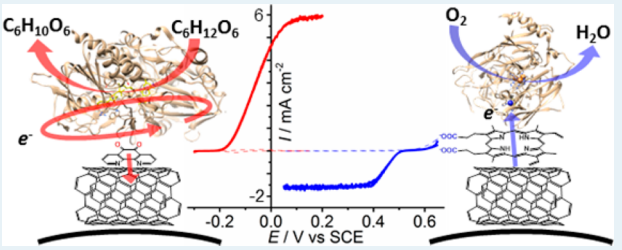
A High Power Buckypaper Biofuel Cell: Exploiting 1,10-Phenanthroline-5,6-dione with FAD-Dependent Dehydrogenase for Catalytically-Powerful Glucose Oxidation

Andrew. J. Gross,* Xiaohong Chen, Fabien Giroud, Caroline Abreu, Alan Le Goff, Michael Holzinger, and Serge Cosnier*

Department of Molecular Chemistry, UMR CNRS-UGA 5250, Université Grenoble Alpes, 38000 Grenoble, France

Supporting Information

ABSTRACT: Enzymatic biofuel cells generate electrical energy from renewable sources with high selectivity and environmental benefits compared to lithium batteries and traditional fuel cells. For enzymatic fuel cells to become competitive, major improvements in electrode design are required to enhance power density, voltage output, and stability. Here we have developed a freestanding paper biofuel cell comprising redox molecule embedded multiwalled carbon nanotube papers for electrical wiring of enzymes. The drop-coat and one-pot fabrication methods provide flexibility and permit easy scalability of functionalized bioelectrodes via commercially available materials. Buckypaper functionalized with 1,10-phenanthroline-5,6-dione (PLQ) as an efficient electron mediator for fungal-derived FAD-dependent glucose dehydrogenase (FADGDH) shows very high steady-state current densities for glucose oxidation of I_{max} = 5.38 ± 0.54 mA cm^{-2} at 0.15 V vs SCE at neutral pH. When coupled with a bioinspired protoporphyrin IX buckypaper cathode, the resulting glucose/O_2 fuel cell delivered a power density of 0.65 ± 0.1 mW cm^{-2} or 24.1 ± 4.7 mW cm^{-3} at a cell voltage of 0.5 V, limited by the cathode. Galvanostatic and current discharge experiments confirm robust short-term operational performance.



KEYWORDS: *bioelectrocatalysis, biocatalyst, paper electrode, enzymatic, FAD-GDH, multicopper oxidases*

INTRODUCTION

Enzymatic biofuels (EBFCs) convert chemical energy into electrical energy under mild conditions from the oxidation of organic fuels such as sugars and alcohols, coupled with the reduction of oxygen using redox enzymes as bioelectrocatalysts.[1−3] Biofuel cells offer several advantages over lithium batteries and traditional fuel cells, including the use of renewable, low-cost, and safe fuels from ecological sources and operation at neutral pH and ambient temperature. Furthermore, EBFCs can operate as membraneless fuel cells owing to the high selectivity of enzymes. Particular attention of biofuel cells over the past decade has been directed toward the use of EBFCs as micropower sources which harvest energy from biological fluids for implantable medical devices.[4−7] In recent years, EBFCs have been successfully implanted in rats,[4] lobsters,[5] and snails.[6] Application of EBFCs for portable and wearable devices is more feasible and has enormous potential. For example, epidermal and contact-lens biofuel cells which harvest energy from sweat or tears using carbon nanotube based electrodes have started to emerge.[8−10] Lightweight biofuel cells with small form factors offer the prospect of self-powered chemical sensors with in situ detection and remediation of toxic chemicals.[11,12]

Specific challenges in EBFC electrode design include the development of electrodes which offer (i) stable immobilization of enzymes and mediators with high loadings, (ii) efficient electron transfer between the active sites of enzymes and the electrode, and (iii) fast mass transport and (iv) are lightweight and easily integrated into devices. To achieve the practical application of biofuel cells, a rapidly emerging approach is to use flavin adenine dinucleotide-dependent glucose dehydrogenase (FADGDH) for catalytic oxidation of glucose at the anode. The FADGDH enzyme offers major advantages for biofuel cells compared to other popular FAD-dependent enzymes such as the gold standard glucose oxidase (GOx).[13,14] Unlike GOx, FADGDH is oxygen insensitive, which prevents consumption of valuable oxygen at the anode. In situ production of hydrogen peroxide, which can be toxic to single compartment fuel cells, is also avoided.[14] However, the commercially available fungal FADGDH does not have the cytochrome-complex subunit for direct electron transfer (DET) with electrodes.[15] As such, the fungal FADGDH requires an artificial electron transfer mediator, which can result in kinetic and thermodynamic losses compared to DET.[16] The identification of high performance mediators is vital for fungal FADGDH for both biofuel cell and sensor applications. Few systems for mediated electron transfer with FADGDH have been investigated and are mainly based on osmium,[13,17−19] ruthenium,[20] and ferro-

Received: March 7, 2017
Revised: May 15, 2017
Published: May 22, 2017

ACS Publications © XXXX American Chemical Society

DOI: 10.1021/acscatal.7b00738
ACS Catal. XXXX, XXX, XXX−XXX

cene[14,21] redox complexes and polymers. These mediators have high redox potentials and slow mediator exchange due to structural rigidity and require complicated synthesis from toxic precursors. Compared to metal-based mediators, small organic mediators with fast mediator exchange are attractive. For example, 1,2 and 1,4 naphthoquinones[22,23] and phenothiazines[24,25] are commonly exploited and give high catalytic currents at attractively low formal redox potentials.

Carbon nanotubes (CNTs) offer great advantages for bioelectrodes and are typically deposited onto an electrode support to give a large surface area with good stability and conductivity.[26] CNT-supported electrodes tend to be heavy, bulky, and not easily miniaturizable.[27,28] Free-standing buckypaper electrodes prepared by vacuum filtration of CNT suspensions on the other hand are thin and lightweight and offer the possibility to immobilize catalysis-promoting aromatic molecules by π-stacking interactions.[29−32] However, such paper electrodes are often fragile with limited conductivity and slow electron transfer kinetics compared to conventional bulk electrodes such as glassy carbon (GC). Further improvements in fabrication methods are required toward CNT paper electrodes with excellent homogeneity, reproducibility, and electrochemical properties.

In this study, we report the preparation of new redox molecule embedded buckypapers for bioelectrocatalysis using four different types of commercially available redox molecules. The focus of the study is the development of high performance catalytic buckypaper bioelectrodes for enzyme wiring without the use of a supporting substrate or polymer scaffold. The use of 1,10-phenanthroline-5,6-dione (PLQ) as a small electron mediator for the fungus-derived FADGDH is explored, and the resulting buckypaper anode integrated into a fully freestanding paper glucose/O_2 biofuel cell with a protoporphyrin buckypaper cathode. Notably, our approach here uses PLQ as a small organic mediator and nanotube binder and therefore avoids polymer and metal complex synthesis. This is in contrast to the structurally and electronically different Ru polymer mediator with PLQ ligands reported previously.[20]

EXPERIMENTAL SECTION

Materials and Apparatus. Monosodium phosphate monohydrate (NaH_2PO_4, ≥98%), disodium hydrogen phosphate heptahydrate (Na_2HPO_4, 98−102%), *N*,*N*-dimethylformamide (DMF, 99.9%), potassium ferricyanide, 1,10-phenanthroline-5,6-dione (PLQ, 97%), protoporphyrin IX (PP, ≥95%, ferriprotoporphyrin IX (FePP, ≥98.0%), 1,4 naphthoquinone (NQ, 97%), potassium chloride (KCl, 99%), D-(+)-glucose (≥99.5%), sodium citrate (>99%), sodium chloride (NaCl, 99.8%), copper chloride ($CuCl_2$, 97%), hydrogen peroxide (H_2O_2, 30 wt % in H_2O), ethylenediaminetetraacetic acid (EDTA, 99%), and sulfuric acid (95−98%) were purchased from Sigma-Aldrich and used as received. Bilirubin oxidase (BOD, 1.2 U mg^{-1}) from *Myrothecium sp.* and flavin adenine dinucleotide-dependent glucose dehydrogenase (FADGDH, 1150 U mg^{-1} solid) from *Aspergillus sp.* were purchased from Amano (Japan) and Sekisui Diagnostics (UK), respectively, and used as received. Enzymes were stored at −20 °C. Distilled water was obtained by water purification to a resistivity of 15 MΩ cm using a Millipore Ultrapure system. Commercial grade multiwalled carbon nanotubes (MWCNTs, Ø = 9.5 nm, 1.5 μm length, ≥95% purity) were obtained from Nanocyl and used as received without purification. High purity oxygen and argon were obtained from Messer. Glucose solutions were left to mutarotate overnight to β-D-glucose prior to use.

Preparation of Unmodified MWCNT Buckypaper and Redox-Embedded MWCNT Buckypaper Electrodes by Drop-Coat Method. First, a 1 mg mL^{-1} MWCNT suspension was prepared by the addition of 150 mg of nonfunctionalized MWCNTs into 150 mL of DMF. The dispersion was then sonicated for 30 min prior to use. After vigorous shaking for 1 min, 66 mL of the suspension was filtered through a Millipore PTFE filter (JHWP, 0.45 μm pore size, Ø = 46 mm) using a vacuum pump, washed with distilled water, and left for 1 h. After filtration, the resulting unmodified buckypaper with Ø = 35 mm was left to dry at room temperature. The buckypaper was obtained after its careful removal from the filter paper, then cut into individual electrodes with Ø = 10 mm (geometric surface area of 0.785 cm^{-2}) using a metal cutter. To obtain functionalized MWCNT buckypaper electrodes, 150 μL of 0.6 mmol L^{-1} or 10 mmol L^{-1} modifier (PP and FePP) in DMF was drop-coated onto unmodified buckypaper surfaces with Ø = 10 mm (each electrode contains 5.39 mg of MWCNTs) and the resulting electrode left to dry overnight at room temperature. Electrical contact was obtained via a metal wire with carbon paste. The back and sides of the electrode were sealed with silicone paste.

Preparation of Redox-Embedded MWCNT Buckypaper Electrodes by One-Pot Method. A 1 mg mL^{-1} MWCNT suspension was first prepared by the addition of 150 mg of nonfunctionalized MWCNTs into 150 mL of DMF. The dispersion was then sonicated for 30 min prior to addition of the modifier (PLQ, NQ, PP, and FePP). The modifier, dissolved in a minimum volume of DMF, was slowly added into the MWCNT suspension to give a final 0.6 mmol L^{-1} or 2 mmol L^{-1} modifier concentration. Prior to filtration, the resulting suspension was sonicated for a further 30 min. After rigorous shaking for 1 min, 66 mL of the suspension was filtered, washed, and dried (as above for the unmodified buckypaper) and the resulting buckypaper cut into electrodes with Ø = 10 mm. Electrical contact was obtained via a metal wire with carbon paste. The back and sides of the electrode were sealed with silicone paste.

Preparation of Buckypaper Bioelectrodes. First, 5 mg mL^{-1} stock solutions of BOD and FADGDH were prepared in 0.1 mol L^{-1} phosphate buffer at pH 7.0 and McIlvaine buffer at pH 7.0 (0.2 mol L^{-1} Na_2HPO_4, 0.1 mol L^{-1} citric acid), respectively. A total of 150 μL of 5 mg mL^{-1} enzyme solution (0.75 mg enzyme) was then added to the surface of a buckypaper with Ø = 10 mm, and the enzyme solution was allowed to fully absorb at 4 °C overnight. The electrode was subsequently rinsed with the corresponding buffer before use.

Electrochemistry. Electrochemical measurements were performed at room temperature using an Eco Chemie Autolab PGSTAT 100 potentiostat running GPES 4.9 software or a Biologic VMP3Multi Potentiostat with EC-lab software. For half-cell testing, a conventional three-electrode cell setup was used comprising a buckypaper working electrode (Ø = 10 mm), a saturated calomel reference electrode (SCE with sat. KCl), and a Pt wire counter-electrode. The complete fuel cell setup comprised a one-pot protoporphyrin buckypaper with BOD biocathode (BP_{PP}-BOD) and a one-pot phenanthroline quinone buckypaper with FADGDH (BP_{PLQ}-FADGDH) bioanode immersed in 20 mL of McIlvaine buffer at pH 7.0 with an interelectrode distance of 3 mm. Gas flows were set qualitatively and moderately to obtain reproducible conditions.

DOI: 10.1021/acscatal.7b00738
ACS Catal. XXXX, XXX, XXX−XXX

Average catalytic current densities were obtained by subtracting the background current: the signal obtained without oxygen, for the cathode, and without glucose, for the anode. Fuel cell experiments were performed by recording a linear sweep polarization from the open circuit voltage (OCV) to 0.02 V with the anode connected to the counter and reference leads, and the cathode connected to the working lead. Power densities were obtained by dividing the power delivery by the surface area or volume of one electrode.

Scanning Electron Microscopy. Buckypaper electrodes with Ø = 3 mm were imaged using a FEI/Quanta FEG 250 scanning electron microscope (Hillsboro, OR, USA) operating at an accelerating voltage of 5 kV without metal coating.

Static Water Contact Angles. Water contact angles were obtained at room temperature by delivering a 2 μL droplet of distilled water onto the sample surface on a horizontal stage using a Dataphysics OCA 35 system. Multiple droplet measurements (8 or 9) were recorded per sample type.

RESULTS AND DISCUSSION

Characterization of Unmodified MWCNT and Redox-Embedded MWCNT Buckypaper Electrodes. Pristine freestanding buckypaper prepared from filtration of CNT dispersions without additives tends to be fragile and difficult to manipulate. Our initial experiments established that the ability to handle pristine unmodified BP was improved when the amount of MWCNTs in the final product was increased by at least a factor of 2.[30] Redox-embedded BP was subsequently prepared in several steps (see Experimental Section) either by the addition of redox molecules to the MWCNTs dispersion before filtration (one-pot method) or after filtration by drop-coating onto the unmodified BP (drop-coat method). The BP functionalization is based on $\pi-\pi$ stacking interactions between aromatic groups and CNT sidewalls. For all buckypapers, flat and reproducible disks were obtained after filtration (Figure 1A), drying, and cutting (Figure 1B and C, respectively). BP thicknesses ranged between 230 and 320 μm (see Table S1). The variability in thickness results from differences in vacuum pressure and the MWCNTs dispersion.

Scanning electron microscopy was performed to evaluate the morphology of unmodified BP (BP, Figure 1D) and BP prepared from the one-pot method with redox molecules: protoporphyrin IX (BP_{PP}, Figure 1E), ferriprotoporphyrin IX (BP_{FePP}, Figure 1F), and 1,10-phenanthroline-5,6-dione (BP_{PLQ}, Figure 1G). The SEM images reveal that the BPs comprise a random and entangled network of MWCNTs with nanoscale porosity. The images show subtle evidence that functionalized BPs have a flatter and more compact topography compared to unmodified BP, suggestive of more intimate interactions between nanotubes in the presence of redox molecules via $\pi-\pi$ stacking.

Cyclic voltammograms (CVs) of the $Fe(CN)_6^{3-}$ redox probe recorded at unmodified and BP_{PP} paper electrodes reveal a significant increase in peak current with a decrease in peak-to-peak separation (ΔE_p) following modification with protoporphyin molecules (see Figure S1). The dramatic enhancement with chemical functionalization is partially attributed to a physical improvement in the electronic connectivity between carbon nanotubes. The increase in peak current observed is also partially attributed to improved diffusion of $Fe(CN)_6^{3-/4-}$ in the 3D-structured electrode, facilitated by the increased surface hydrophilicity (Figure S2).

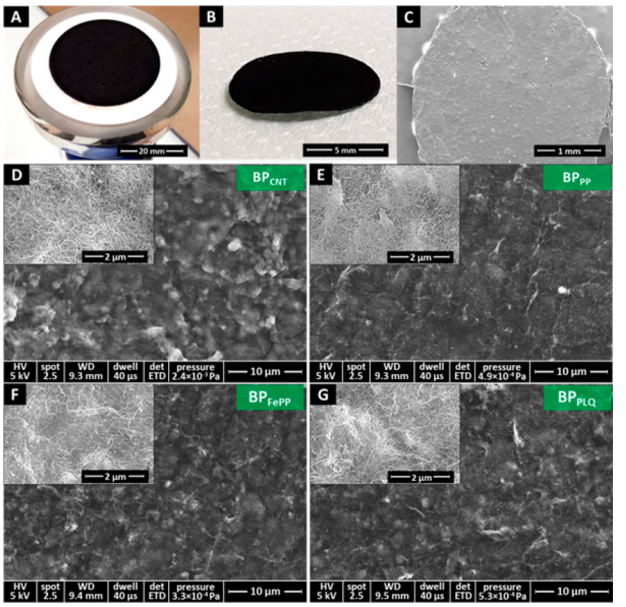


Figure 1. (A, B) Photographs of freshly prepared BP_{PP} buckypaper (A) after filtration and (B) after filtration, drying, and cutting into the electrode. (C–G) SEM micrographs of (C, E) BP_{PP}, (D) BP, (F) BP_{FePP}, and (G) BP_{PLQ} buckypaper electrodes recorded at (C) 60×, (D–G) 5000× and 40 000× (inset) magnification. All modified electrodes were prepared by the one-pot method.

To investigate the presence and accessibility of porphyrin and PLQ molecules in BP prepared via the one-pot and drop-coat methods, cyclic voltammetry was performed on one-sided BP samples with a geometric surface area of 0.785 cm^2. CVs were first recorded at functionalized electrodes prepared by the one-pot method in argon-saturated 0.1 mol L^{-1} phosphate buffer at pH 7.0. Figure 2 shows CVs recorded at BP_{FePP} and BP_{PLQ} prepared via the one-pot method. The CVs reveal the presence of well-defined chemically reversible processes. At BP_{FePP}, the one-electron Fe^{III}/Fe^{II} redox couple is observed at $E_{1/2}$ = −0.38 V vs SCE (10 mV s^{-1}), consistent with reported

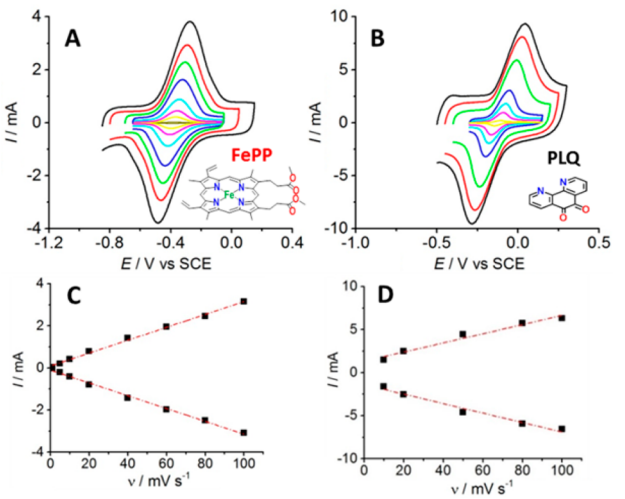


Figure 2. (A,B) CVs recorded at (A) BP_{FePP} and (B) BP_{PLQ} buckypaper electrodes (one-pot method) in Ar saturated 0.1 mol L^{-1} phosphate buffer at pH 7 at different scan rates. (C, D) Corresponding plots of anodic and cathodic peak current versus scan rate.

DOI: 10.1021/acscatal.7b00738
ACS Catal. XXXX, XXX, XXX–XXX

Table 1. Electrochemical Parameters for BP_{FePP} and BP_{PLQ} Electrodes Prepared by One-Pot and Drop-Coating Functionalization Methods

buckypaper electrode (number[a])	fabrication method	modifier concentration (mmol L^{-1})	surface concentration[b] (10^{-7} mol cm^{-2})	ΔE_p (mV)	$E_{1/2}$ (V)
BP_{FePP} (n = 3)	one-pot	0.6	1.38 ± 0.58	65	−0.37
BP_{FePP} (n = 3)	drop-coat	0.6	0.48 ± 0.25	55	−0.35
BP_{FePP} (n = 7)	drop-coat	10	6.43 ± 3.58	215	−0.36
BP_{PLQ} (n = 3)	one-pot	2	1.21 ± 0.30	118	−0.13

[a]Number of independent buckypaper electrode samples analyzed. [b]Surface concentrations obtained from the anodic peak of CVs recorded at 10 mVs^{-1} in Ar.

values of $E_{1/2}$ = −0.34 V and −0.39 V vs SCE for FePP modified MWCNTs on GC.[33,34] At BP_{PLQ}, the two-electron two-proton o-quinone/o-hydroquinone system is observed at $E_{1/2}$ = −0.13 V vs SCE (10 mV s^{-1}) as previously observed for PLQ adsorbed on MWCNTs on GC electrodes.[35]

Well-defined voltammograms and a linear dependence (r^2 > 0.95) of peak current on scan rate for anodic and cathodic peaks are observed at the BP_{FePP} and BP_{PLQ} electrodes (Figure 2C and D), confirming that the redox molecules are accessible and surface bound. The stability of the immobilized molecules was tested by subjecting the electrodes to repeat potential cycling at 20 mV s^{-1} (Figure S3). No noticeable loss in electroactivity was observed after 20 cycles, confirming the high stability of the immobilized redox groups and the bulk nanotube structure despite the noncovalent modification approach.

Modified BP_{FePP} electrodes prepared by the drop-coat method were also examined by voltammetry and gave the expected electroactivity as observed for the one-pot method. BP_{FePP} electrodes were prepared by drop-coating 150 μL of 0.6 mmol L^{-1} or 10 mmol L^{-1} FePP DMF solutions onto pristine unmodified BPs (Ø = 10 mm). The electrochemical parameters obtained from CVs recorded in phosphate buffer at pH 7.0 and 10 mV s^{-1} are listed in Table 1.

Examination of the data in Table 1 reveals that one-pot BP_{FePP} exhibits a higher surface concentration than drop-coat BP_{FePP} (1.38 ± 0.58 versus 0.48 ± 0.25 × 10^{-7} mol cm^{-2}) when the same initial modifier concentration is used, consistent with effective bulk functionalization via the one-pot method. Increasing the modifier concentration from 0.6 mmol L^{-1} to 10 mmol L^{-1} resulted in a very high surface concentration of 6.43 ± 3.58 × 10^{-7} mol cm^{-2}, highlighting the possibility to tailor redox molecule loading in the paper electrodes. It is expected that such high surface concentrations would be possible via the one-pot method with a 10 mmol L^{-1} modifier concentration. However, this was not explored due to the high volumes and quantity of modifier required for one-pot buckypaper fabrication. The surface concentrations for FePP prepared here are significantly higher than previously reported values of 6.8 × 10^{-10} mol cm^{-2} and 1.1 × 10^{-9} mol cm^{-2} for FePP modified MWCNTs on GC.[33,34] The high loadings observed here are consistent with an effective high surface area 3D-structured matrix.

Table 1 also reveals that BP_{FePP} prepared via one-pot and drop-coat methods with 0.6 mmol L^{-1} modifier solution give similar peak-to-peak separation values of ≤65 mV and therefore similar apparent electron transfer kinetics. Significantly larger ΔE_p values and therefore sluggish electron transfer kinetics were observed for highly functionalized BP_{FePP} electrodes prepared with 10 mmol L^{-1} of the modifier. This is consistent with an extensive network of redox molecules being deeply embedded in the CNT structure, which would increase electron tunneling distances and film resistivity.

On the basis of the BP_{FePP} optimization experiments, we prepared PLQ buckypaper via the one-pot method using a modestly high concentration of 2 mmol L^{-1}. No further optimization was performed. The surface concentration obtained for one-pot BP_{PLQ} was 1.21 ± 0.30 × 10^{-7} mol cm^{-2}, which reveals the possibility to obtain high redox molecule loadings with a near 1 × 10^{-7} mol cm^{-2} concentration. The ΔE_p value of 118 mV observed for BP_{PLQ} is consistent with a slow rate of electron transfer, increased BP resistivity, and a large degree of potential inversion for the two-electron two-proton quinone process.[36]

Bioelectrocatalytic O_2 Reduction at BP_{pp} Electrodes with Immobilized BOD Enzyme from *Myrothecium verrucaria*. For biocathode construction, the multicopper oxidase (MCO) enzyme BOD from *Myrothecium verrucaria* (*Mv*) was employed as the catalyst for the four-electron reduction of O_2 to H_2O. BOD is a promising enzyme for biofuel cells due to its high bioelectrocatalytic activity under mild conditions and formal potential close to that of the O_2/H_2O couple (0.816 V vs RHE at pH 0). Bilirubin, as a natural substrate for BOD, and its analogues, have been attached to MWCNT electrodes to facilitate DET with *Mv*BOD for O_2 reduction.[34,37] The interaction is supported by favorable immobilization and orientation. However, a commonly accepted problem with BOD is that significant catalytic activity loss is observed in the presence of H_2O_2, a common byproduct of oxidase enzymes found in glucose/O_2 biofuel cells. The use of O_2-insensitive FADGDH in biofuel cell design can circumvent this issue.

In this study, the porphyrin-BOD system was exploited for the development of buckypaper cathodes. One-pot BP_{pp} electrodes were first prepared then incubated with BOD, washed with phosphate buffer at pH 7.0, then tested for enzyme presence and activity. Figure 3A and B show CVs recorded in argon and oxygen at one-pot BP_{PP}-BOD and BP-BOD, respectively. Under oxygen, both types of electrode exhibited similar onset potential of E_{onset} = 0.54 ± 0.01 V vs SCE and 0.52 ± 0.01 V vs SCE, respectively. The onset potentials are close to that of the predicted T1 copper site of *Mv*BOD responsible for substrate oxidation and successive electron transfers ($E_{1/2(T1)}$ = 0.48 V vs SCE at pH 7.0).[34] The onset potentials are close to the ideal thermodynamic reduction potential for O_2 of 0.572 V vs SCE at pH 7.0 (assuming a potential difference of 244 mV between RHE and SCE reference electrodes). The onset potential values are therefore very attractive for biofuel cell applications and consistent with efficient single-proton single-electron DET between the BP and the enzyme.

The catalytic wave observed in oxygen at BP_{PP} confirms DET accompanied by the electrocatalytic reduction of oxygen via

DOI: 10.1021/acscatal.7b00738
ACS Catal. XXXX, XXX, XXX−XXX

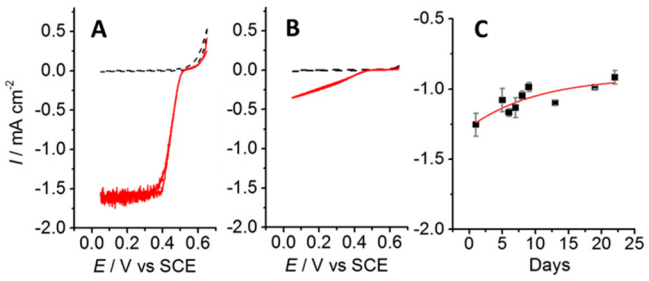


Figure 3. (A,B) CVs of bioelectrocatalytic O_2 reduction recorded at (A) BP_{PP} (one-pot method) and (B) BP buckypaper electrodes after BOD enzyme immobilization in (--) Ar saturated and (−) O_2 saturated 0.1 mol L^{-1} phosphate buffer at pH 7.0 at scan rate = 0.2 mV s^{-1}. (C) Evolution of maximum catalytic current density as a function of time for BP_{PP}-BOD. Chronoamperograms recorded at E_{app} = 0.2 V vs SCE and current densities obtained after 30 min. Error bars correspond to one standard deviation from two electrodes.

BOD. On the basis of repeat measurements, an average maximum current density of 0.34 ± 0.15 mA cm^{-2} is observed at BP compared to 1.33 ± 0.17 mA cm^{-2} for BP_{PP} (one-pot method), confirming substantially enhanced performance for the protoporphyrin buckypaper. At BP, an ill-defined "residual slope" current is observed in oxygen, attributed to unfavorable orientation of adsorbed enzymes. In contrast, at the BP_{PP} electrode, well-defined steady-state voltammograms are observed consistent with fast mass transport, enzyme catalysis, and heterogeneous electron transfer at the buckypaper electrode.[37] It is noted that a scan rate of 0.2 mV s^{-1} was employed due to the superior steady-state signals with low capacitance (see Figure S4 for catalytic currents recorded at different scan rates). A summary of the catalytic parameters obtained at different bioelectrodes is shown in Table 2.

Table 2. Catalytic Parameters for BP_{PP}-BOD Cathode and BP_{PLQ}-FADGDH Anode Prepared by One-Pot and Drop-Coating Functionalization Methods

buckypaper electrode (number[a])	fabrication method (modifier concentration)	onset potential (V)[b]	maximum catalytic current (mA cm^{-2})[b,c]
BP_{PP}-BOD (n = 5)	one-pot (0.6 mmol L^{-1})	0.54 ± 0.01	1.33 ± 0.17
BP_{PP}-BOD (n = 3)	drop-coat (0.6 mmol L^{-1})	0.54 ± 0.01	1.10 ± 0.14
BP_{PP}-BOD (n = 3)	drop-coat (10 mmol L^{-1})	0.54 ± 0.01	1.26 ± 0.11
BP-BOD (n = 3)	unmodified	0.52 ± 0.01	0.34 ± 0.15
BP_{PLQ}-FADGDH (n = 5)	one-pot (2 mmol L^{-1})	−0.23 ± 0.01	5.38 ± 0.54
BP-FADGDH (n = 2)	unmodified	−0.01 ± 0.00	0.002 ± 0.001

[a]Number of independent buckypaper electrode samples analyzed. [b]Parameters obtained from the forward sweep of CVs recorded at 0.2 mV s^{-1}. [c]Current obtained at 0.2 and 0.15 V at BOD and FADGDH electrodes, respectively.

The long-term stability of BP_{PP}-BOD was also assessed by periodically recording chronoamperograms at E_{app} = 0.2 V vs SCE for 30 min over 24 days of storage in phosphate buffer at pH 7.0 (Figure S5). The corresponding plot in Figure 3C of the maximum catalytic current obtained on different days reveals remarkable stability for BP_{PP}-BOD, with the current density decreasing by 10% over the first 7 days and 27% over 24 days. Stability experiments performed in a similar manner at other MWCNT-MCO enzyme cathodes report 40−45% current loss after 1 week and 45−60% after 20−24 days.[38,39] To clarify, such stability experiments evaluate both operational stability (for 30 min per day) and storage stability. The enhanced stability observed here compared to that with CNT-modified GC electrodes is consistent with improved physical enzyme entrapment into the nanopore-containing CNT matrix via fixation and/or dynamic reorganization effects.[40]

A brief assessment of the bioelectrocatalytic performance of BP_{PP}-BOD was also performed to demonstrate enzyme inhibition at the biocathode. CVs recorded in the presence and absence of 40 mmol L^{-1} H_2O_2 in phosphate buffer at pH 7.0 in oxygen are shown in Figure S6 and clearly reveal the loss of oxygen reduction current due to inhibition of immobilized bilirubin oxidase by H_2O_2. The catalytic current was suppressed in the presence of H_2O_2 and remained suppressed after transfer to a fresh phosphate buffer solution, confirming that the enzyme's activity was inhibited and not restored. The absence of oxygen reduction in these experiments validates the importance of the active "wired" enzyme as the biocatalyst. Chronoamperometry performed at BP_{PP}-BOD in phosphate buffer at pH 7.0 in oxygen (Figure S6) revealed the rapid nature of enzyme inhibition by H_2O_2 and the good stability of the biocathode in the presence of a physiologically relevant concentration of NaCl (100 mM).

The bioelectrocatalytic performance of BP_{PP} for oxygen reduction was also performed at electrodes prepared by the drop-coat method. No significant difference in E_{onset} was observed between drop-coat and one-pot BP_{PP} electrodes. Likewise, equivalent sigmoidal steady-state current responses (with different current magnitudes) were observed for all BP_{PP} electrodes. For drop-coat BP_{PP}, the maximum average catalytic current only slightly increased from 1.10 ± 0.14 to 1.26 ± 0.11 mA cm^{-2} with an increase in protoporphyrin modifier from 0.6 mmol L^{-1} to 10 mmol L^{-1}.

The best performing biocathode identified here was the BP_{PP}-BOD prepared using the one-pot method with I_{max} = 1.33 ± 0.17 mA cm^{-2}. The high performance of this biocathode is clear given that typical values obtained by our group and others for CNT paper-based MCO cathodes are 0.17 to 1.1 mA cm^{-2} in oxygen-saturated solution.[27,29,30,41,42]

Bioelectrocatalytic Glucose Oxidation at BP_{PLQ} Electrodes with Immobilized FADGDH from *Aspergillus sp.* For bioanode development, the one-pot method was exploited for preparation of a new type of redox-embedded buckypaper with immobilized FADGDH. To prepare the anode, a MWCNT dispersion containing 2 mmol L^{-1} of 1,10-phenanthroline-5,6-dione (PLQ) was used. The bioanode was obtained by drop-casting 150 μL of 5 mg mL^{-1} enzyme solution onto the BP_{PLQ} and leaving the solution overnight until the droplet had fully adsorbed. The PLQ molecule has previously been reported as a mediator for the cofactors NADH/NADPH coupled with NAD/NADP-dependent enzymes.[35,43] To the best of our knowledge, the phenanthroline quinone as a free ligand has not been demonstrated as a mediator for FAD-dependent enzymes such as FADGDH. In addition to the low redox potentials, a major advantage of phenanthroline quinone mediators is their nonreactivity toward active-site enzyme amine and thiol groups.[43] In this work, we have investigated the use of PLQ, in the form of a redox-embedded functionalized buckypaper, to electrically connect

DOI: 10.1021/acscatal.7b00738
ACS Catal. XXXX, XXX, XXX−XXX

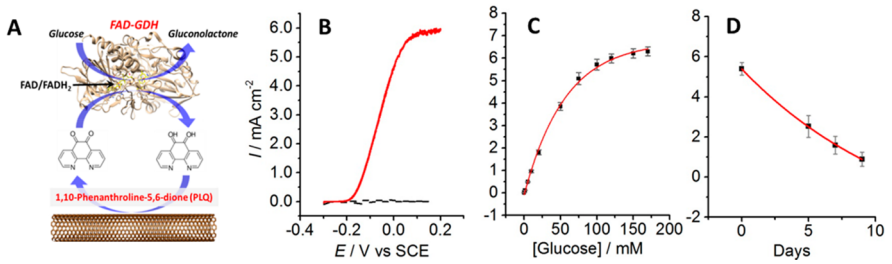


Figure 4. (A) Scheme illustrating bioelectrocatalytic oxidation of glucose on BP_{PLQ} buckypaper via MET with the active site of FADGDH. (B) CVs recorded at a BP_{PLQ} buckypaper electrode after FADGDH immobilization in (--) 0 mmol L^{-1} and (−) 170 mmol L^{-1} glucose in Ar saturated McIlvaine buffer at pH 7.0 at scan rate = 0.2 mV s^{-1}. (C) Plot of average current density obtained for different glucose concentrations recorded at three BP_{PLQ}-FADGDH electrodes. (D) Evolution of maximum catalytic current density as a function of time for BP_{PLQ}-FADGDH with 170 mmol L^{-1} glucose. (C, D) Chronoamperograms recorded at E_{app} = 0.15 V vs SCE and current densities obtained after 30 min. Error bars correspond to one standard deviation from at least two electrodes.

the active site of FADGDH to the electrode for bioelectrocatalytic oxidation of glucose (see Figure 4A). In this mechanism, the FADGDH oxidizes the β-D-glucose to D-glucono-1,5-lactone using the FAD cofactor, which itself is reduced to $FADH_2$. The PLQ mediator then acts as a secondary electron acceptor to oxidize the reduced cofactor, $FADH_2$. The mediator is finally reoxidized by the electrode which is set at an appropriate oxidizing potential.

Figure 4B and Figure S7 show CVs recorded in 0 (--) and 170 mmol L^{-1} (−) glucose in McIlvaine buffer at pH 7.0 at one-pot BP_{PLQ}-FADGDH and BP-FADGDH electrodes, respectively. In the presence of 170 mmol L^{-1} glucose, an onset potential of E_{onset} = −0.23 ± 0.01 V vs SCE is observed at BP_{PLQ}-FADGDH, which is attractively low for a glucose-oxidizing bioanode and similar to that obtained using 1,4 naphthoquinone hydrogel mediators with FADGDH (E_{onset} = −0.18 to −0.25 V vs SCE at near neutral pH).[22,23] Interestingly, the onset potential of −0.23 V is much more negative than the ≈−0.05 V previously reported using a Ru-PLQ polymer with FADGDH,[20] highlighting an advantage of using the free PLQ mediator in this form. The onset potential is around 180 mV positive of the estimated redox potential of −0.41 V vs SCE for the enzyme-bound relay, $FAD/FADH_2$, consistent with thermodynamically attractive electron wiring.[22] The onset potential at BP_{PLQ} for glucose oxidation is also about 200 mV more negative than ferrocene and osmium mediator-modified electrodes with E_{onset} ≈ −0.05 to 0.15 V vs SCE,[17,19,21] and thus PLQ is an attractive mediator for biofuel cell applications.

The voltammograms recorded at BP_{PLQ} under argon in the absence and presence of 170 mmol L^{-1} glucose clearly demonstrate a drastic increase in current signal with glucose addition. Well-defined sigmoidal waves are observed at 0.2 mV s^{-1} consistent with electrocatalytic oxidation of glucose. A maximum current density of 5.38 ± 0.54 mA cm^{-2} is observed at 0.15 V at BP_{PLQ} without stirring. In contrast, voltammograms recorded at BP under the same conditions reveal a negligible maximum current density of 0.002 ± 0.001 mA cm^{-2}. The substantial enhancement in catalytic current provides compelling evidence for mediated electron transfer reaction via PLQ. The high catalytic currents obtained were subsequently validated by comparison with a CNT paper prepared using a known mediator for FADGDH. A 1,4 naphthoquinone buckypaper, BP_{NQ}-FADGDH, was prepared and tested in the same manner as for BP_{PLQ}-FADGDH. Voltammetry revealed a significantly smaller maximum current density of 2.20 mA cm^{-2} (Figure S8). Despite being less powerful than the BP_{PLQ} electrode, the BP_{NQ} electrode still exceeds recent high performance NQ-anodes.[22,23]

The catalytic current obtained of 5.38 ± 0.54 mA cm^{-2} at 0.15 V vs SCE for BP_{PLQ} in unstirred solution exceeds the performance of that observed at most bioanodes to date without the use of hydrodynamic conditions. We believe that the BP_{PLQ} anode exhibits the highest catalytic density for glucose oxidation of any paper-based bioanode. At phenothiazine-modified commercial buckypaper with immobilized NAD-dependent GDH and NAD cofactor, current densities up to 2.6 mA cm^{-2} at 25 °C have been reported.[25] With the addition of 1 mmol L^{-1} NAD^+ in solution, the catalytic current increased to 4.5 mA cm^{-2} at a high potential of 0.35 V. In addition to the high potential required, the use of NAD in solution is less convenient than if the cofactor is surface-bound or enzyme-bound. High performing bioanode architectures typically produce no more than 2 mA cm^{-2} [22,44,45] with the exception of a hierarchical porous carbon bioelectrode which exibited enormous densities up to 100 mA cm^{-2} with rapid convection.[18] With CNT-modified Toray papers with immobilized glucose oxidase and dehydrogenases, current densities in the range 1−3.3 mA cm^{-2} have been reported.[23,46−48]

Evaluation of the steady-state current at a fixed potential of 0.15 V as a function of glucose concentration reveals a linear increase in the range 1 mmol L^{-1} to 50 mmol L^{-1} (see calibration plot in Figure S9). As a side note, the linearity of r^2 = 0.996 and the ability to detect beyond the upper limit of 30 mmol L^{-1} means that the BP_{PLQ}-FADGDH meets basic requirements for a commercial glucose sensor.

Figure 4C shows that the steady-state currents increased with increasing concentration to a plateau at 170 mmol L^{-1} glucose; hence 170 mmol L^{-1} was adopted in experiments as the concentration to maximize catalytic current output, limited by the enzymatic reaction and catalyst surface coverage. Limiting current values were reached within 30 s (Figure S10), consistent with fast mass transport of glucose at the electrode. Estimated values for the apparent Michaelis−Menten and velocity constants of K_m = 40.4 mmol L^{-1} and V_{max} = 6.1 mA cm^{-2}, respectively, are obtained. The estimated K_m is similar to that observed for fungal FADGDHs (K_m = 35 mmol L^{-1} [49]), and hence the BP_{PLQ} electrode maximizes electrocatalysis without significantly affecting the enzymes' binding constant for glucose.

The stability of the BP_{PLQ}-FADGDH bioanode was assessed over 10 days by periodically recording chronoamperograms at E_{app} = 0.15 V vs SCE for 30 min in McIlvaine buffer at pH 7.0 (Figure S11). The plot in Figure 4D of the maximum catalytic

DOI: 10.1021/acscatal.7b00738
ACS Catal. XXXX, XXX, XXX−XXX

current obtained on different days reveals that the bioanode is significantly less stable than the biocathode. After 2 days, 75% of the original current remains. After 5 days, only 48% of the initial current remains. Similar storage stability for an FADGDH electrode has previously been observed using an Os polymer mediator with 80% of the initial current observed after 2 days followed by a rapid breakdown to 56% after 6 days.[13] This finding suggests that PLQ may be no less toxic or inhibitory toward FADGDH than osmium polymers. Despite the poor stability, high maximum current densities of ≈1 mA cm^{-2} are nevertheless possible after 10 days, confirming that the BP_{PLQ} is operational for several days.

Assessment of the bioelectrocatalytic performance of BP_{PLQ}-FADGDH was also performed to explore enzyme inhibition at the bioanode. CVs recorded before and after the addition of 10 mmol L^{-1} of $CuCl_2$ in McIlvaine buffer at pH 7.0 are shown in Figure S12 and clearly reveal the loss of glucose oxidation current due to inhibition of immobilized FADGDH, attributed to binding of Cu^{2+} to the $FADH_2$ cofactor as previously observed for glucose oxidase.[50] The possibility to reverse the enzyme inhibition by addition of a strong metal chelator to reverse binding of the metal ions to FAD was also tested. The voltammogram obtained after addition of an excess of ethylenediaminetetracetic acid (EDTA, 11 mmol L^{-1}) and mild stirring shows an increase in the catalytic oxidation current on the reverse sweep, attributed to partial reactivation of the biocatalyst.

Single Compartment Biofuel Cell with a BP_{PP}-BOD Cathode and BP_{PLQ}-FADGDH Anode Prepared via One-Pot Fabrication. Power generation from membraneless glucose/oxygen biofuel cells using redox-embedded bucky-papers was subsequently investigated. A single-compartment glucose/O_2 paper-based biofuel cell was constructed using a BP_{PP}-BOD cathode and a BP_{PLQ}-FADGDH anode prepared via one-pot methods (Figure 5A). Linear polarization curves were recorded at 0.2 mV s^{-1} in McIlvaine buffer at pH 7.0 to evaluate the performance under oxygen-saturated (≈ 1.1 mmol L^{-1}) and quiescent oxygen conditions (≈ 0.23 mmol L^{-1}) with 170 mmol L^{-1} glucose.[51] Large OCVs of 0.74 ± 0.01 V and 0.67 ± 0.01 V were obtained under quiescent and oxygen-saturated conditions, respectively. The OCVs match closely the estimated maximum voltage of 0.77 V from the half-cell polarization experiments. The difference in OCV between the quiescent and oxygen-saturated conditions is attributed to a small amount of degradation between fuel cell testing experiments.

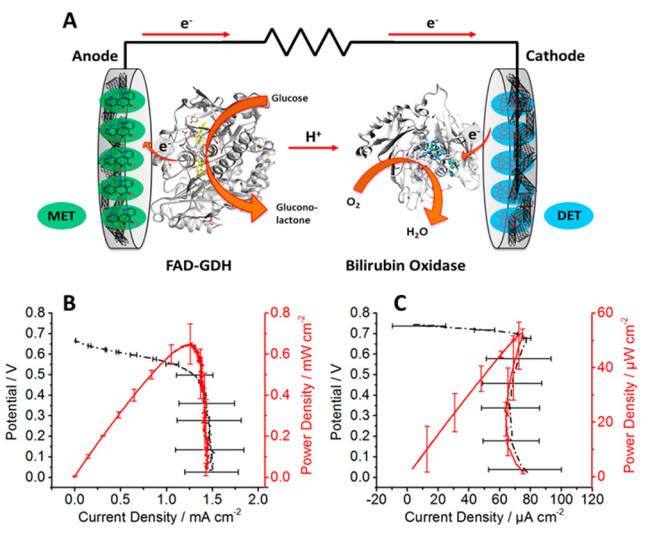


Figure 5. (A) Scheme illustrating the single compartment buckypaper biofuel cell comprising an O_2 reducing BP_{PP}-BOD cathode and glucose oxidizing BP_{PLQ}-FADGDH anode. (B, C) Biofuel cell polarization (---) and power curves (—) recorded under (B) oxygen-saturated and (C) quiescent oxygen conditions in McIlvaine buffer at pH 7.0 with 170 mmol L^{-1} glucose. Polarization voltammograms were recorded at 0.2 mV s^{-1}. Error bars correspond to one standard deviation from three biofuel cells.

Average polarization and power curves (Figure 5B and C) reveal a maximum power density of 0.65 ± 0.10 mW cm^{-2} or 24.07 mW cm^{-3} at 0.5 V for the biofuel cell under oxygen-saturated conditions without stirring. Under quiescent oxygen with no stirring, a maximum power density of 0.053 mW cm^{-2} or 1.97 mW cm^{-3} is observed. The power outputs for these glucose/O_2 biofuel cells are either very good or exceptional depending on whether the power delivery is divided by the surface area (cm^2) or volume (cm^3). It is noted that we used equal sized anodes and cathodes in this work and that the power densities were obtained by dividing the power delivery by either the surface area or volume of one electrode. Given that buckypaper is a three-dimensional electrode and size is a crucial parameter for portable biofuel cell applications, the power density in mW cm^{-3} is arguably more appropriate. However, for this work we have chosen to remain with the standard mW cm^{-2} convention for figures. Maximum power outputs for a single EBFC in the literature are between 1.45 and 2.3 mW cm^{-2} at 0.3 to 0.55 V.[22,23,52] One of these previously reported biofuel cells, based on our estimates, gives up to 3.8 mW cm^{-3} (1.54 mW cm^{-2} [52]), and thus the delivery of 24.07 mW cm^{-3} reported here is markedly high.

The difference in power density observed between the saturated and quiescent oxygen conditions reveals that the biofuel cell is strongly limited by oxygen availability at the cathode. Even in the presence of oxygen-saturated conditions, the biocathode is limiting.

Polarization and power curves were also recorded at freshly prepared biofuel cells in the absence of glucose under oxygen-saturated conditions as control experiments (Figure S13). In the absence of the enzyme's substrate, the low power output and a small OCV, namely 0.02 mW cm^{-2} and 0.53 ± 0.02 V, clearly illustrate and confirm the unambiguous role of FADGDH and the need for glucose for effective biofuel cell performance.

In order to assess the operational stability of the biofuel cell, potentiostatic and galvanostatic tests were performed for 30 min. This duration may, for example, be considered as an adequate operational time for a single use self-powered biosensor. The stability of the biofuel cell was first examined by applying a mild fixed voltage of 0.2 V and monitoring the current in oxygen-saturated solution. The power obtained from the recorded current revealed a stable power output of 295 ± 25 μW cm^{-2} after an initial 30 s induction period (Figure 6A). Similar glucose/oxygen biofuel cell stability has been observed using FADGDH, which, notably, is vastly superior to that observed with the GOx enzyme.[14] The initial induction period is attributed to diffusional equilibration and high charging currents. To further assess the stability, a current of 500 μA was continuously drawn and the evolution of voltage monitored (Figure 6B). Following the short initial induction period, a stable voltage of 0.57 ± 0.01 V is obtained.

DOI: 10.1021/acscatal.7b00738
ACS Catal. XXXX, XXX, XXX−XXX

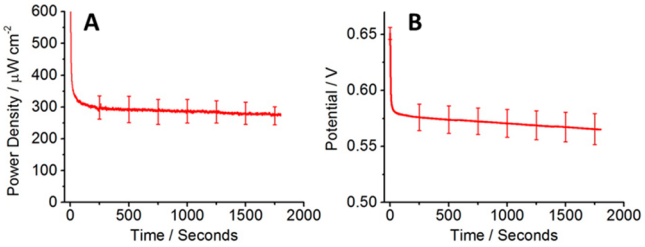


Figure 6. (A) Power generated from current discharge at 0.2 V and (B) voltage generated at 600 μA cm^{-2} (500 μA) for 30 min operation of the BP_{PP}-BOD/BP_{PLQ}-FADGDH biofuel cell in O_2 saturated McIlvaine buffer at pH 7.0 with 170 mmol L^{-1} glucose. Error bars correspond to one standard deviation from three biofuel cells.

CONCLUSIONS

Electricity generation from glucose and oxygen using small and lightweight enzymatic biofuel cells opens up the attractive prospect of self-powered health and environmental sensor devices. Here, we report the fabrication of new freestanding redox-embedded (porphyrin, phenanthroline quinone, and napthoquinone) carbon nanotube paper electrodes with physical durability, practical flexibility, and excellent electrochemical properties. Elaboration of the electrodes for construction of bioelectrodes with high catalytic performance compared to literature values was subsequently demonstrated. Very high catalytic performance was observed by employing 1,10-phenanthroline-5,6-dione as an electron transfer mediator with FADGDH at the anode. The biofuel cell delivers milliwatt per cubic centimeter power densities under either quiescent solution (dissolved oxygen) or saturated oxygen solution conditions, with 170 mmol L^{-1} glucose at neutral pH and room temperature. In addition, the half-cell and biofuel cell experiments show good operational stability, which could be appropriate for disposable self-powered sensors. We expect that the proposed fabrication methods, buckypapers, and use of PLQ for mediated electron transfer with FADGDH will advance the field of biofuel cells toward practical applications, especially considering the excellent prospects of the FADGDH enzyme and paper-based bioelectrodes. Future work is now required to address the limiting cathode power output under quiescent oxygen levels (for example, by enhancement of dioxygen mass transport) and the comparatively poor stability observed at the anode over several days (for example, via caging and shrinking effects).

ASSOCIATED CONTENT

Supporting Information

The Supporting Information is available free of charge on the ACS Publications website at DOI: 10.1021/acscatal.7b00738.

Electrode characterization and stability, Figures S1−S13 (PDF)

AUTHOR INFORMATION

Corresponding Authors

*E-mail: andrew.gross@univ-grenoble-alpes.fr.
*E-mail: serge.cosnier@univ-grenoble-alpes.fr.

ORCID

Andrew. J. Gross: 0000-0002-7356-7089
Xiaohong Chen: 0000-0002-6535-3873
Alan Le Goff: 0000-0002-6765-5859
Michael Holzinger: 0000-0003-3700-4673

Author Contributions

The manuscript was written through contributions of all authors. All authors have given approval to the final version of the manuscript.

Notes

The authors declare no competing financial interest.

ACKNOWLEDGMENTS

This work was supported by LabEx ARCANE (ANR-11-LABX-0003-01) and ANR-15-JTIC-0002-01. The region Auvergne-Rhône-Alpes is acknowledged for the Ph.D. funding of C.A. The authors would also like to thank the platform Chimie NanoBio ICMG FR 2607 (PCN-ICMG) and PFT "Surfaces Functionalization and Transduction" for providing facilities and PMIEL "Microscopy" for SEM imaging. We are very grateful to Christine Lancelon Pin for assistance with SEM imaging.

REFERENCES

(1) Cosnier, S.; Gross, A. J.; Le Goff, A.; Holzinger, M. *J. Power Sources* **2016**, *325*, 252−263.
(2) Slaughter, G.; Kulkarni, T. *J. Biochips Tissue Chips* **2015**, *5* (111), 1−10.
(3) Agnès, C.; Holzinger, M.; Le Goff, A.; Reuillard, B.; Elouarzaki, K.; Tingry, S.; Cosnier, S. *Energy Environ. Sci.* **2014**, *7*, 1884−1888.
(4) Zebda, A.; Cosnier, S.; Alcaraz, J.-P.; Holzinger, M.; Le Goff, A.; Gondran, C.; Boucher, F.; Giroud, F.; Gorgy, K.; Lamraoui, H.; Cinquin, P. *Sci. Rep.* **2013**, *3*, 370−375.
(5) MacVittie, K.; Halámek, J.; Halámková, L.; Southcott, M.; Jemison, W. D.; Lobel, R.; Katz, E. *Energy Environ. Sci.* **2013**, *6*, 81−86.
(6) Halámková, L.; Halámek, J.; Bocharova, V.; Szczupak, A.; Alfonta, L.; Katz, E. *J. Am. Chem. Soc.* **2012**, *134*, 5040−5043.
(7) Cinquin, P.; Gondran, C.; Giroud, F.; Mazabrard, S.; Pellissier, A.; Boucher, F.; Alcaraz, J.-P.; Gorgy, K.; Lenouvel, F.; Mathé, S.; Porcu, P.; Cosnier, S. *PLoS One* **2010**, *5*, e10476.
(8) Jia, W.; Valdés-Ramírez, G.; Bandodkar, A. J.; Windmiller, J. R.; Wang, J. *Angew. Chem., Int. Ed.* **2013**, *52*, 7233−7236.
(9) Ogawa, Y.; Kato, K.; Miyake, T.; Nagamine, K.; Ofuji, T.; Yoshino, S.; Nishizawa, M. *Adv. Healthcare Mater.* **2015**, *4*, 506−510.
(10) Pankratov, D.; González-Arribas, E.; Blum, Z.; Shleev, S. *Electroanalysis* **2016**, *28*, 1250−1266.
(11) Giroud, F.; Gross, A. J.; Faggion, D., Jr.; Holzinger, M.; Maduro de Campos, C. E.; Acuña, J. J. S.; Domingos, J. B.; Cosnier, S. *J. Electrochem. Soc.* **2017**, *164*, H3052−H3057.
(12) Arechederra, R. L.; Minteer, S. D. *Anal. Bioanal. Chem.* **2011**, *400*, 1605−1611.
(13) Zafar, M. N.; Beden, N.; Leech, D.; Sygmund, C.; Ludwig, R.; Gorton, L. *Anal. Bioanal. Chem.* **2012**, *402*, 2069−2077.
(14) Milton, R. D.; Giroud, F.; Thumser, A. E.; Minteer, S. D.; Slade, R. C. T. *Phys. Chem. Chem. Phys.* **2013**, *15*, 19371−19379.
(15) Shiota, M.; Yamazaki, T.; Yoshimatsu, K.; Kojima, K.; Tsugawa, W.; Ferri, S.; Sode, K. *Bioelectrochemistry* **2016**, *112*, 178−183.
(16) Saboe, P. O.; Conte, E.; Farell, M.; Bazan, G. C.; Kumar, M. *Energy Environ. Sci.* **2017**, *10*, 14−42.
(17) Murata, K.; Akatsuka, W.; Sadakane, T.; Matsunaga, A.; Tsujimura, S. *Electrochim. Acta* **2014**, *136*, 537−541.
(18) Tsujimura, S.; Murata, K.; Akatsuka, W. *J. Am. Chem. Soc.* **2014**, *136*, 14432−14437.
(19) Pinyou, P.; Ruff, A.; Poeller, S.; Ma, S.; Ludwig, R.; Schuhmann, W. *Chem. - Eur. J.* **2016**, *22*, 5319−5326.
(20) Sakuta, R.; Takeda, K.; Ishida, T.; Igarashi, K.; Samejima, M.; Nakamura, N.; Ohno, H. *Electrochem. Commun.* **2015**, *56*, 75−78.
(21) Milton, R. D.; Lim, K.; Hickey, D. P.; Minteer, S. D. *Bioelectrochemistry* **2015**, *106*, 56−63.
(22) Hou, C.; Lang, Q.; Liu, A. *Electrochim. Acta* **2016**, *211*, 663−670.

DOI: 10.1021/acscatal.7b00738
ACS Catal. XXXX, XXX, XXX−XXX

(23) Milton, R. D.; Hickey, D. P.; Abdellaoui, S.; Lim, K.; Wu, F.; Tan, B.; Minteer, S. D. *Chem. Sci.* **2015**, *6*, 4867−4875.
(24) Ravenna, Y.; Xia, L.; Gun, J.; Mikhaylov, A. A.; Medvedev, A. G.; Lev, O.; Alfonta, L. *Anal. Chem.* **2015**, *87*, 9567−9571.
(25) Narváez Villarrubia, C. W.; Artyushkova, K.; Garcia, S. O.; Atanassov, P. *J. Electrochem. Soc.* **2014**, *161*, H3020−H3028.
(26) Cosnier, S.; Holzinger, M.; Le Goff, A. *Front. Bioeng. Biotechnol.* **2014**, *2*, 2296−4185.
(27) Bunte, C.; Hussein, L.; Urban, G. A. *J. Power Sources* **2014**, *247*, 579−586.
(28) Narvaez Villarrubia, C. W.; Soavi, F.; Santoro, C.; Arbizzani, C.; Serov, A.; Rojas-Carbonell, S.; Gupta, G.; Atanassov, P. *Biosens. Bioelectron.* **2016**, *86*, 459−465.
(29) Bourourou, M.; Elouarzaki, K.; Holzinger, M.; Agnès, C.; Le Goff, A. L.; Reverdy-Bruas, N.; Chaussy, D.; Party, M.; Maaref, A.; Cosnier, S. *Chem. Sci.* **2014**, *5*, 2885−2888.
(30) Gross, A. J.; Robin, M. P.; Nedellec, Y.; O'Reilly, R. K.; Shan, D.; Cosnier, S. *Carbon* **2016**, *107*, 542−547.
(31) Elouarzaki, K.; Bourourou, M.; Holzinger, M.; Le Goff, A.; Marks, R. S.; Cosnier, S. *Energy Environ. Sci.* **2015**, *8*, 2069−2074.
(32) Reuillard, B.; Warnan, J.; Leung, J. J.; Wakerley, D. W.; Reisner, E. *Angew. Chem., Int. Ed.* **2016**, *55*, 3952−3957.
(33) Reuillard, B.; Gentil, S.; Carrière, M.; Le Goff, A. L.; Cosnier, S. *Chem. Sci.* **2015**, *6*, 5139−5143.
(34) Lalaoui, N.; Le Goff, A.; Holzinger, M.; Cosnier, S. *Chem. - Eur. J.* **2015**, *21* (47), 16868−16873.
(35) Faggion, D. F., Jr.; Haddad, R.; Giroud, F.; Holzinger, M.; Maduro de Campos, C. E. M. de; Acuña, J. J. S.; Domingos, J. B.; Cosnier, S. *Nanoscale* **2016**, *8*, 10433−10440.
(36) Kim, R. S.; Chung, T. D. *Bull. Korean Chem. Soc.* **2014**, *35*, 3143−3155.
(37) So, K.; Kitazumi, Y.; Shirai, O.; Kano, K. *J. Electroanal. Chem.* **2016**, *783*, 316−323.
(38) Lalaoui, N.; Rousselot-Pailley, P.; Robert, V.; Mekmouche, Y.; Villalonga, R.; Holzinger, M.; Cosnier, S.; Tron, T.; Le Goff, A. *ACS Catal.* **2016**, *6*, 1894−1900.
(39) Bourourou, M.; Elouarzaki, K.; Lalaoui, N.; Agnès, C.; Le Goff, A.; Holzinger, M.; Maaref, A.; Cosnier, S. *Chem. - Eur. J.* **2013**, *19*, 9371−9375.
(40) Gutierrez-Sanchez, C.; Ciaccafava, A.; Blanchard, P. Y.; Monsalve, K.; Giudici-Orticoni, M. T.; Lecomte, S.; Lojou, E. *ACS Catal.* **2016**, *6*, 5482−5492.
(41) Hussein, L.; Rubenwolf, S.; von Stetten, F.; Urban, G.; Zengerle, R.; Krueger, M.; Kerzenmacher, S. *Biosens. Bioelectron.* **2011**, *26*, 4133−4138.
(42) Scherbahn, V.; Putze, M. T.; Dietzel, B.; Heinlein, T.; Schneider, J. J.; Lisdat, F. *Biosens. Bioelectron.* **2014**, *61*, 631−638.
(43) Forrow, N. J.; Sanghera, G. S.; Walters, S. J.; Watkin, J. L. *Biosens. Bioelectron.* **2005**, *20*, 1617−1625.
(44) de Souza, J. C. P.; Iost, R. M.; Crespilho, F. N. *Biosens. Bioelectron.* **2016**, *77*, 860−865.
(45) Cadet, M.; Gounel, S.; Stines-Chaumeil, C.; Brilland, X.; Rouhana, J.; Louerat, F.; Mano, N. *Biosens. Bioelectron.* **2016**, *83*, 60−67.
(46) Ivnitski, D.; Branch, B.; Atanassov, P.; Apblett, C. *Electrochem. Commun.* **2006**, *8*, 1204−1210.
(47) Reid, R. C.; Giroud, F.; Minteer, S. D.; Gale, B. K. *J. Electrochem. Soc.* **2013**, *160*, H612−H619.
(48) Hickey, D. P.; Reid, R. C.; Milton, R. D.; Minteer, S. D. *Biosens. Bioelectron.* **2016**, *77*, 26−31.
(49) Sakai, G.; Kojima, K.; Mori, K.; Oonishi, Y.; Sode, K. *Biotechnol. Lett.* **2015**, *37*, 1091−1099.
(50) Meredith, M. T.; Minteer, S. D. *Anal. Chem.* **2011**, *83*, 5436−5441.
(51) Yomo, T.; Urabe, I.; Okada, H. *Anal. Biochem.* **1989**, *179*, 124−126.
(52) Reuillard, B.; Le Goff, A.; Agnès, C.; Holzinger, M.; Zebda, A.; Gondran, C.; Elouarzaki, K.; Cosnier, S. *Phys. Chem. Chem. Phys.* **2013**, *15*, 4892−4896.

DOI: 10.1021/acscatal.7b00738
ACS Catal. XXXX, XXX, XXX−XXX